RSC Advances

ROYAL SOCIETY OF CHEMISTRY

www.rsc.org/advances

Effect of Acid-leaching on Carbon-supported Copper Phthalocyanine Tetrasulfonic Acid Tetrasodium Salt (CuTSPc/C) for Oxygen Reduction Reaction in Alkaline Electrolyte: the active site studies

Qing Zhang[1], Taishan Zhu[2], Xin Qing[2], Jinli Qiao[1,2*], Shuhui Sun[3*]

[1]*School of Chemistry and Chemical Engineering, Key Laboratory of Green Chemical Media and Reactions, Ministry of Education, Henan Normal University, Xinxiang, Henan 453007, P. R. China*

[2]*College of Environmental Science and Engineering, Donghua University, 2999 Ren'min North Road, Shanghai 201620, P. R. China*

[3]*Institut National de la Recherche Scientifique (INRS), Energie Materiaux Telecommunications Research Center 1650 Boul. Lionel-Boulet Varennes, Quebec, J3X 1S2 (CANADA)*

*Corresponding author. Tel: +86-21-67792379. Fax: +86-21-67792159. E-mail: qiaojl@dhu.edu.cn, shuhui@emt.inrs.ca

Effect of Acid-leaching on Carbon-supported Copper Phthalocyanine Tetrasulfonic AcidTetrasodium Salt (CuTSPc/C) for Oxygen Reduction Reaction in Alkaline Electrolyte: the active site studies

Qing Zhang[a], Taishan Zhu[b], Xin Qing[b], Jinli Qiao[a,b]*, Shuhui Sun[c]*

Abstract: Although the non-precious metal catalysts (NPMCs) have been extensively studied as low-cost catalyst alternatives to Pt, particular to oxygen reduction reaction (ORR) in polymer electrolyte membrane fuel cells (PEMFCs), the nature of the active ORR catalytic sites is still a subject of controversy. In this work, using carbon supported copper phthalocyanine tetrasulfonicacid tetrasodium salt (CuTSPc/C) nanoparticles as target catalyst, the effects of transition metal Cu on ORR active sites are systematically studied by both rotating disk electrode (RDE) and rotating ring disk electrode (RRDE) techniques in alkaline electrolyte. The results show that acid-leaching can significantly decrease the ORR activity of the CuTSPc/C catalyst, with half-wave potential negatively shifted by more than 50 mV compared to the catalyst before acid-leaching. The electron transfer number of the ORR process catalyzed by the catalyst before acid-leaching was kept for about 3.85 during the whole tested potential range from -0.6 ~ -0.1V, while this number greatly decreased from 3.82 at -0.55V to 3.53 at -0.1V after acid-leaching. The H_2O_2 produced accordingly increased sharply from 7.8% to 22%. XRD and TEM results indicate that acid-leaching is an effective method to remove metal-Cu. XPS analysis reveal that metal Cu is essential in the ORR active site structure, and also plays a key part in the stabilization of the active N and S species.

Keywords: Copper phthalocyanine; oxygen reduction reaction; acid-leaching; active site

1. Introduction

Increasing energy demanding and environmental pollution have stimulated significant research into new, efficient and sustainable energy sources to compensate for and even replace traditional ones [1,2]. In this regard, the proton-exchange membrane (PEM) fuel cells have evoked great attention as a promising green energy device due to their several advantages such as high energy efficiency, high energy/power densities, and low/zero emissions [3-5]. To date, the slow cathodic oxygen reduction reaction (ORR) kinetics with larger overpotential (or polarization) have been identified as the major barrier in a fuel cell [6]. To make PEM fuel cell technically feasible and practical, in the current state of technology, Pt-based catalysts must be used to catalyze the slow ORR due to their high catalytic performances for both the anode and cathode. However, as Pt-based catalysts have insufficient electrochemical durability and come at a high cost [6-8], the major efforts in PEM fuel cells research and development have been put on reducing Pt loading by exploring more active catalysts, and/or replacing Pt metal using other non-precious metals such as Fe, Co and Cu [9,10]. In spite of this progress, very few show the real promise to comparable Pt since the requirements for both good ORR activity and stability are difficult to be achieved for normal non-noble catalysts in such a strong acidic condition for PEM fuel cell operation.

Recently, the growing interest in the application of alkaline fuel cells (AFCs) is principally motivated by the prospective use of cheap, easy to start, and relatively abundant non-precious metal catalysts (NPMCs) [11-13]. In a basic environment, the catalyst activity toward ORR is much higher, and the improved materials stability is highly afforded, thus leading to a reduced Pt loading and extended choices for suitable Pt alternatives [11-13]. In particular, extensive work have been done to develop transition metal N-containing complexes, conductive polymer-based catalysts, transition metal chalcogenides, metaloxides/carbides/nitrides/oxynitrides/carbonitrides and enzymatic compounds [14-18]. Among these NPMCs, pyrolyzed metal-nitrogen materials supported on

carbon (M-N_X/C) are considered as the most promising ORR catalysts, especially for Fe- and/or Co-based ones [11,14,19]. As yet, the ORR activities of this kind of non-precious metal catalysts are still insufficient. Although some methods and materials have widely been used to produce active non-precious metal ORR catalysts, there are still difficulties in discerning the controlling parameters in preparing active catalysts. There is a general agreement in the literature that kinds of transition metal, nitrogen, type of carbon support and pyrolysis process are all have effects on the catalyst's ORR activity and stability [20-23]. Among these four factors, the nitrogen and carbon support are considered to be essential for the active sites. Regarding the role of the metal ion in the catalytic process, however, there has two different views: (i) the presence of metal ions plays important role in the formation of active sites (M-N_x/C, X=2 or 4) [24-26]; (ii) the transition metal does not act as part of active site, instead it is only helping to facilitate the stable incorporation of nitrogen into the graphitic structure of carbon, and the formation of active carbon during high-temperature pyrolysis [27].

To form N-containing non-precious metal catalysts for the ORR, metal phthalocyanines (MPcs) have been explored as the catalyst precursors due to their unique delocalized conjugated bond with eight N atoms in a unit structure, making MPcs liable to oxidation and reduction [21,28-32]. In particular, the pyrolyzed Co- and Fe-centered phthalocyanines have been proven to be the most promising catalysts, which exhibit remarkable ORR activities close to that of commercially available Pt/C catalyst [21,28,29]. On the other hand, there has also been found that the ORR activity of MPcs strongly depend on central metal ions [22,30] and the pH value of electrolyte [31]. For example, Sehlotho *et al*. found that MnPc complexes could catalyze a 2-electron transfer ORR in acidic media, but 4-electron transfer one in alkaline media [31]. Most recently, we have demonstrated the excellent ORR activities of carbon-supported copper phthalocyanine (CuPc), which even surpasses the pyrolyzed CoPc/C in alkaline condition [32]. For a continuing effort, we further report that metal Cu, nitrogen and sulfur could be simultaneously formed onto the carbon support framework to form new Cu-N-S/C catalysts by pyrolyzing a carbon supported copper

phthalocyanine tetrasulfonic acid tetrasodium salt (CuTSPc/C) nanoparticle catalysts, without additional dopant precursor [33]. As shown in Table 1, in the use of EDX-mapping data for exploring the active site structure, an interesting phenomenon can be seen: the nitrogen content in catalysts has no significant decline with an increase in heat-treatment temperature. This suggests that the presence of Cu and S species could prevent phthalocyanine from thermal decomposition and contribute to higher nitrogen content during the pyrolysis process (where the more nitrogen concentration in the catalyst synthesis could benefit the catalyst's ORR activity). Moreover, S has also been proven to be an essential part of ORR active site, and the synergetic effect between N and S could be spontaneously formed within the catalyst [33]. Nevertheless, the role of transition metal playing in the catalysts' active sites is still unclear.

Inspired by the results achieved in our continuing effort, in this work, with carbon-supported copper phthalocyanine tetrasulfonic acid tetrasodium salt (CuTSPc/C) nanoparticles as the target catalyst, the role of central metal Cu ion in macrocycle complex was investigated by an acid-leaching model. The catalytic ORR activities of the catalysts before and after acid-leaching were studied thoroughly by linear sweep voltammetry (LSV) employing rotating disk electrode (RDE) and rotating ring-disk electrode (RRDE) techniques in 0.1 M KOH. The ORR kinetic parameters and possible reaction mechanisms were discussed. For fundamental understanding, the XRD, TEM and XPS analyses were also performed to identify the surface structure change and the possible active sites of these catalysts before and after acid-leaching.

2. Experimental

2.1 Materials and catalyst preparation

Copper phthalocyanine tetrasulfonic acid tetrasodium salt (CuTSPc) was provided by Sigma Aldrich with 60% purity and used as both the metal precursor and nitrogen precursor. In this work, the Vulcan XC-72R carbon black was used as carbon

support, which was purchased from Cobat Corporation with 236.8 m^2g^{-1} specific surface area. Carbon-supported copper phthalocyanine tetrasulfonic acid tetrasodium salt catalysts (CuTSPc/C) were prepared via a combined solvent-impregnation and milling procedure along with high-temperature treatment. In detail, the preparation was processed by combining a mixture of 40 mg CuTSPc and 60 mg carbon black in a mortar, milling by adding 10 ml methanol for 2h, and then was vacuum-dried at 40°C for 1h to remove methanol. The resulting catalyst were further placed in a quartz boat and pyrolyzed at 700°C for 120 min at a rate of 20°C min^{-1} in a flowing nitrogen atmosphere. This catalyst as-prepared is thus designated as $(CuTSPc/C)_{700}$. In order to remove the metal Cu, the catalyst was further disposed with an acid-leaching procedure after heat-treatment. In detail, the $(CuTSPc/C)_{700}$ catalyst was refluxed in 0.5M H_2SO_4 at 80°C for 8h, then the suspension was washed with deionized (D.I.) water and centrifuged until the supernatant to be neutral. The catalyst powder obtained was finally dried at 60°C in an oven overnight under ambient air conditions, which was then designated as $(CuTSPc/C)_{700}$AL.

2.2 Physical characterizations

The microstructures of both $(CuTSPc/C)_{700}$ and $(CuTSPc/C)_{700}$AL catalysts were examined by X-ray power diffraction (XRD), transmission electron microscopy (TEM) and X-ray photoelectron spectroscopy (XPS). XRD measurements were carried out on a Philips PW3830 X-ray diffractometer equipped with Cu-Ka radiation (λ = 0.15406 nm). The current was 40 mA and the voltage was 40 kV. The intensity data were collected at 25°C in the 2θ range from 0° to 90° with a scan rate of 1.20$^o min^{-1}$. TEM was performed on JEM-2100F operated at an acceleration voltage of 200 kV to obtain information of the average particle size and the distribution of the catalyst prepared. XPS analysis was carried out on a Kratos AXIS Ultra^{DLD} electron spectrometer with Al K X-ray anode source ($h\nu$ = 1486.6eV) at 250W and 14.0 kV. The XPS Peak 41 software was used for fitting the XPS spectrum.

2.3 *Electrochemical measurements*

All the electrochemical measurements were carried out in a conventional three-electrode cell using CHI760D electrochemical workstation controlled at room temperature. The electrocatalytic activities of both $(CuTSPc/C)_{700}$ and $(CuTSPc/C)_{700}AL$ catalysts were evaluated by linear sweep voltammetry (LSV) using a rotating disk electrode (RDE) and a rotating ring-disk electrode (RRDE) techniques. A glassy carbon (GC) electrode (a diameter of 5.615 mm corresponding to a geometric surface area of 0.2475 cm^2, purchased from Pine Instruments) was used as the working electrode. Prior to use, the GC electrode surface was polished with Al_2O_3 (0.05 μm) suspension and rinsed with D.I. water. The catalyst ink was prepared by mixing 25 mg of the catalyst with 2 ml of isopropyl alcohol to form a mixture, which was then ultrasonically dispersed for 45 minutes to dissolve as evenly as possible. Then 10 μL of the catalyst ink was deposited onto the GC electrode surface, leading to a catalyst loading of 0.5 mg cm^{-2}. After drying at room temperature, one drop of methanol/Nafion® solution (50:1 wt%) was dropped onto the top of the catalyst layer to improve adhesion during the electrochemical measurement.

RDE experiments were performed in a three-electrode electrochemical cell, and 0.1M KOH was used as the electrolyte at room temperature. A saturated calomel electrode (SCE) and platinum wire were used as reference and counter electrodes, respectively. All measured potentials were referenced to a standard hydrogen electrode (SHE). Linear sweep voltammetry (LSV) in O_2-saturated 0.1M KOH were measured at 1500 rpm with a sweep rate of 5 mV s^{-1} and a potential range between -0.6 and 0.3 V. To verify the ORR catalytic pathways of the catalyst, the RRDE measurements were performed to monitor the formation of peroxide species during the ORR process.

3. Results and Discussion

3.1 Oxygen reduction reaction activity

According to the literatures, the "metal-free" catalysts are normally considered to exhibit better stability than transition metal N-containing complexes because there are no issues related to metal dissolution and poisoning as observed from those metal-containing catalysts [34-36], and the acid-leaching (the heated H_2SO_4) are usually used for removing the transition metal ions during the catalysts synthesis [37,38]. However, there has no any report on the acid-leaching used for the pyrolyzed macrocyclic structured metal phthalocyanines. Fig. 1 shows the ORR polarization curves of CuTSPc/C catalyst electrode before and after acid-leaching, which are measured in O_2-saturated 0.1M KOH at room temperature, respectively. One can see that the $(CuTSPc/C)_{700}$ catalyst gives the onset potential at 0.18V and a half-wave potential ($\Delta E_{1/2}$) at 0.04V, along with a better-defined diffusion-limiting current plateau ranging from -0.2～-0.6V. This suggests that the distribution of active sites on $(CuTSPc/C)_{700}$ electrode is uniform and the oxygen reduction reaction rate is fast enough. Compared to $(CuTSPc/C)_{700}$ catalyst, on the contrary, the $(CuTSPc/C)_{700}$AL catalyst exhibited the onset potential at 0.13V with a half-wave potential ($\Delta E_{1/2}$) at 0.00V, ie., after acid-leaching the electrocatalytic activity of the catalyst decreased greatly, where the half-wave potential of $(CuTSPc/C)_{700}$AL is negatively shifted by more than 50 mV compared to $(CuTSPc/C)_{700}$. In addition, the good current plateau as observed for $(CuTSPc/C)_{700}$ electrode was also destroyed to some extent, particular in the high-polarization range. The above results indicate that acid-leaching procedure has negative effect on the ORR activity. Since the aim of acid-leaching in this work is to remove the central metal Cu, it can be concluded that the presence of metal-Cu might be beneficial for promoted more active sites for the oxygen reduction of $(CuTSPc/C)_{700}$ catalysts as will be discussed below.

For a further comparison of the catalytic ORR activity of CuTSPc/C catalyst before and after acid-leaching, the mass-corrected Tafel plots of log j_k (mA cm^{-2}) vs. the electrode potential E are constructed in Fig. 1(b), on both $(CuTSPc/C)_{700}$ and $(CuTSPc/C)_{700}$AL electrodes. These Tafel curves were deduced from the polarization

curves of Fig. 1(a) with a rotation rate of 1500 rpm. It can be clearly seen that the Tafel slopes for $(CuTSPc/C)_{700}$ catalyst can be divided into two parts, i.e., about 77.6 mV dec^{-1} at the lower overpotential region (E < 150 mV vs. SHE.) and about 127.8 mV dec^{-1} at the higher overpotential region (E < 50 mV vs. SHE.), implying a 1-electron process involved in the rate-determining step [24]. On the contrary, the Tafel slope of $(CuTSPc/C)_{700}$AL catalyst is high above 185.7 mV dec^{-1} at the higher overpotential region, where E < -50 mV vs. SHE. These data clearly indicate that the ORR mechanism strongly depends on the electrode materials (ie., the acid-leading process) investigated in this work, as also put in evidence by the different number of electrons involved in the ORR.

It is known that the electrochemical reduction of oxygen is a multi-electron reaction that has two main possible pathways: one involving gain of $2e^-$ to produce H_2O_2, and the other, a direct $4e^-$ pathway to produce water. In PEMFCs operation, the favorite ORR process is expected to be a 4-electron transfer process from O_2 to H_2O rather than to H_2O_2 in order to obtain the maximum energy capacity. Therefore, for further understanding the catalytic performance of $(CuTSPc/C)_{700}$ catalyst in the absence of Cu, the RRDE measurements were used to quantitatively verify the ORR catalytic pathways of the catalyst after acid-leaching. Based on the RRDE measurements in Fig. 2 (a) and (b), the number of electron transferred (n) and the percentage of H_2O_2 produced can be calculated according to the formulas [26]:

$$n = \frac{4I_d}{I_d + I_r / N} \quad (1)$$

$$\%H_2O_2 = 100 \times \frac{2I_r / N}{I_d + I_r / N} \quad (2)$$

where I_d, I_r and N are the disk current, ring current, and collection efficiency (0.37 in the present work), respectively. According to these equations, we can calculate peroxide species percentage and the number of electron transferred as shown in Fig. 2(c) and (d). It can be seen that $(CuTSPc/C)_{700}$ and $(CuTSPc/C)_{700}$AL both could catalyze the ORR with a 4-electron transfer dominated process. Nevertheless, the electron transfer number of the ORR process catalyzed by $(CuTSPc/C)_{700}$ (ie., before

acid-leaching) was kept for about 3.85 during the whole tested potential range from -0.6 ~-0.1V, whereas this number decreased greatly from 3.82 at -0.55V to 3.53 at -0.1V for $(CuTSPc/C)_{700}AL$) (ie., after acid-leaching). The H_2O_2 produced for the latter thus increased sharply from 7.8% to 22%. In fact, the volatility of these two kinetic parameters (*n* and $\%H_2O_2$) is much larger for the catalyst after acid-leaching than in the case of before acid-leaching. Obviously, the results in Fig. 2 indicate that the presence of metal Cu may not only influence the ORR path, but also may have certain effect on the catalytic stability.

3.2 Morphology and structural characterizations

Fig. 3 Shows the XRD patterns for both $(CuTSPc/C)_{700}$ and $(CuTSPc/C)_{700}AL$ in order to clarify the structure change before and after acid-leaching, which can help us to have a further understanding of the influence mechanisms of acid-leaching on the ORR activity. For both samples, two large broad peaks located at $2\theta = 24.5^o$ and $2\theta = 43.0^o$ are assigned to the (002) and (100) reflection of amorphous carbon support (Vulcan XC-72R) [39,40]. From Fig. 3(a), it is noted that the reflections which would be characteristic for copper particles are not present, instead, the $(CuTSPc/C)_{700}$ catalyst sample shows two better resolved characteristic peaks of sulfated copper(I)-containing compound ($NaCu_2(SO_4)_2OH\ H_2O$) at $2\theta = 31.9^o$ [41] and copper hydroxide ($Cu(OH)_2$) at $2\theta = 34.0^o$ [42], respectively. Also, the reflection around $2\theta < 10^o$, which is associated with the crystalline nature of CuTSPc, was not observed. These results imply that the macrocyclic structure of CuTSPc have been decomposed when the pyrolysis temperature exceeds 700^oC, resulting in the rearrangement of the carbon and nitrogen atoms. However, a large amount of Cu atoms are in the form of Cu-N-S/C structure (which is considered to be the oxygen reduction active site) [33] or compounds rather than a metallic Cu (which are not active for the ORR) (Fig. 3(a)). Very different from $(CuTSPc/C)_{700}$ catalyst sample, the above copper-containing characteristic peaks completely disappeared for $(CuTSPc/C)_{700}AL$ as can be clearly seen in Fig. 3(b), indicating that the metal-Cu

may be removed after acid-leaching. Based on the electrochemical measurement results (Fig. 1 and Fig. 2), this may explain the fact that why we observed higher ORR activity of $(CuTSPc/C)_{700}$ catalyst than that of $(CuTSPc/C)_{700}AL$ catalyst. Combining what will be discussed later, the presence of the metal-Cu might has a great effect on the formation of ORR active site structures as will be further verified by the following TEM analysis.

Fig. 4 shows the typical TEM images for both catalyst samples, which can help us to understand the morphology and particle size differences before and after acid-leaching. It can be seen that for $(CuTSPc/C)_{700}$ catalyst (Fig. 4(a)), some bright particles with size about 20 ~ 30 nm are uniformly distributed on the surface of carbon support. The shape of these particles can also be demonstrated in Fig. 4(b), an enlargement of the area outlined in Fig. 4a. More interestingly, Fig. 4(b) clearly shows the lattice fringe spacing of 1.25 nm, corresponding to the lattice images of the single-crystal copper (002) plane [43], which has never been reported in the literatures as to pyrolyzed metal phthalocyanines. These particles are the Cu-containing cluster compounds (Cu-N-S/C), which is considered to be highly catalytic active for the ORR as has been reported in our recent work [33]. In the case of $(CuTSPc/C)_{700}AL$ catalyst (Fig. 4(c)), however, the TEM image surface only shows agglomerated carbon carrier, and no any Cu-containing particles with crystal structure can be found. Based on the above-mentioned results, it is clear that the structure of Cu-N-S/C was destroyed due to loss of Cu after acid-leaching, which is in a well agreement with what we have observed from XRD results (Fig. 3).

3.3 Active site studies

For further clarifying the possible active sites for the ORR catalyzed by the $(CuTSPc/C)_{700}$ catalysts before and after acid-leaching, XPS analyses are carried out and the results are summarized in Fig. 5. In the full-spectrum analysis, the emissions from C1s, N1s, O1s and S2p levels that constitute the molecules for both $(CuTSPc/C)_{700}$ and $(CuTSPc/C)_{700}AL$ were clearly observed. The element of Cu that

constitutes the molecules of $(CuTSPc/C)_{700}$ was also clearly identified (XPS; see Fig. S1, Supporting Information, SI). However, the peaks of Cu2p were not found after acid-leaching, and the content of Cu is too small to be detected. This can be seen more intuitively in Table 2. As seen more clearly in Fig. 5(a), the Cu 2p spectrum for $(CuTSPc/C)_{700}$ catalyst sample can be de-convoluted into four peaks, except for the higher energy band of Cu 2p spectra which is originated from a broad Cu (II) satellite extending from 940 to 950 eV. The four narrow peaks at 932.4, 933.4, 934.5 and 935.4eV are ascribed to the cuprous species [43-45], copper nitrides [46], copper hydroxide [47,48] and part of undecomposed CuTSPc/C, respectively. Although the peak at 935.4 eV still can be observed but both peak height and peak area decreased significantly. This indicates that most of CuTSPc/C have been decomposed and forms the Cu-N-S/C structure as we observed from XRD pattern. The differences in decomposed content of CuTSPc/C between XPS spectra and XRD pattern is possibly due to the different measurement techniques, and the encapsulation of the precursor into the carbon frameworks below the detection limit of the XRD analysis. As shown in Fig. 5(b), however, the above Cu 2p peaks disappeared totally for $(CuTSPc/C)_{700}$AL sample, and no any fitting peaks can be achieved, indicating that the metal Cu is indeed basically removed after acid-leaching process.

The N1s spectra for both $(CuTSPc/C)_{700}$ and $(CuTSPc/C)_{700}$AL catalyst samples are presented in Fig. 5 (c and d). According to literatures [37,47,49], the peaks of N 1s at 398.6 ± 0.3eV, 400.5 ± 0.3eV and 401.3 ± 0.3eV are corresponding to pyridinic-N, pyrrolic-N and graphitic-N, where both pyridinic-N and graphitic-N are considered as the active sites for ORR. As shown in Fig. 5(c), the N 1s band for $(CuTSPc/C)_{700}$ catalyst can be de-convoluted into four peaks with binding energies of 398.4 eV, 400.0 eV, 400.7 eV and 401.5 eV, respectively. The peak at 400.0 eV can be assigned to C=N [50], while another three peaks are due to pyridinic-N (398.4eV), pyrrolic-N (400.7eV) and graphitic-N (401.5eV), respectively. However, after acid-leaching, only three N 1s bands are observed at 398.9 eV (pyridinic-N), 400.0 eV (C=N) and 400.8 eV (pyrrolic-N), where the graphitic-N totally disappeared as can be clearly seen in Fig. 5(d). Combined with the results obtained from Fig. 1 and 2, if associating

the remarkable ORR activity of $(CuTSPc/C)_{700}$ catalyst with the observed pyridinic-N peak and graphitic-N peak, one may propose that the active sites for ORR is essentially weaken due to loss of Cu during acid-leaching process..

For a more convenient comparison, the content of each types of N (the density of active species) are summarized in Fig. 5(e). It is interestingly to find that although the graphitic-N disappeared in $(CuTSPc/C)_{700}AL$ catalyst, the total concentration of N species increased from 1.60% for $(CuTSPc/C)_{700}$ to 2.07% for $(CuTSPc/C)_{700}AL$ (Table 2). Moreover, the proportion of pyridine-N decreased greatly from 63.1% for $(CuTSPc/C)_{700}$ to 41.1% for $(CuTSPc/C)_{700}AL$ based on the calculation from Fig. 5(e). On the contrary, the proportion of C=N and pyrrolic-N strongly increased, that is, the density of active sites is decreased greatly after acid-leaching. Therefore, it is reasonable to deduce that the disappearing of graphitic-N and the decreasing of pyridine-N lead to a significant degradation of ORR activity on $(CuTSPc/C)_{700}$ catalyst electrode. The presence of pyridinic-N may be the fact that the $(CuTSPc/C)_{700}AL$ catalyst still maintains certain ORR activity even after acid-leaching. In our previous work, we have also found that the total mass loss of CuTSPc/C and CuPc/C is much smaller than that of H_2Pc/C [32,33], indicating that Cu species could effectively prevent phthalocyanine from thermal decomposition, and contribute to higher nitrogen content which if benefit for ORR activity sites. All these facts suggest that the presence of central metal-Cu is not only essential in the ORR active site structure, but also plays a key role in stabilization of N active species. These conclusions also coincide well with what observed from RDE results (Fig. 1).

Fig. 5(f and g) presents the results obtained for the S2p spectral region for catalyst samples before and after acid-leaching. It can be seen that $(CuTSPc/C)_{700}$ catalyst shows a large band ranging from 166.0-172.0 eV, which can be attributed to the formation of sulfated copper-containing compound [51]. Besides, it also exhibits the two primary components at 163.7 eV and 164.9 eV overlapping with each other. The band at 163.7 eV is assigned to $C\text{-}S_n\text{-}C$ structure, and the other band at 164.9 eV is close to that of neutral S (164.5) or the S-S bond (164.6 eV) [33,51]. After acid-leaching, the peak intensity at 167.0-170.0 eV was largely reduced. Meantime,

the peaks at 163.7 eV and 164.9 eV both positively shifted to 163.9 eV and 165.1 eV, indicating some extent of formation of thiophene-S2$p_{3/2}$ and thiophene-S2$p_{1/2}$, respectively [18,48]. In other words, the content of C-S_n-C is decreased due to loss of Cu, and changes to the formation of thiophene-S after acid-leaching process. Calculated from Fig. 5(h), the proportion of thiophene-S2$p_{1/2}$ structure in the total S for the catalyst is about 30%. Based on the observations, we can infer that the some extent of decrease in C-S_n-C and a large decrease in active N species can be the reason of the lower ORR activity of the $(CuTSPc/C)_{700}$AL catalyst than that of $(CuTSPc/C)_{700}$ catalyst. Although the S2$p_{1/2}$ at 165.1 eV is confirmed as the active sulfur component [18,52], the formation of active thiophene-S2$p_{1/2}$ obviously could not make up for the large decreasing of active N species. It is demonstrated further by these facts that the presence of Cu plays a key role in both formation and stabilization of N active species and active C-S_n-C species.

4. Conclusions

In conclusion, the role of central metal Cu ion played in the CuTSPc/C catalyst's ORR active sites was investigated using acid-leaching model. Through electrochemical measurements and the physical characterization analyses, some important results can be obtained: (i) RDE results show that the acid-leaching process has negative effect on ORR activity, where the half-wave potential for $(CuTSPc/C)_{700}$AL catalyst is negatively shifted by more than 50 mV compared to $(CuTSPc/C)_{700}$ sample; (ii) RRDE results indicate that compared to $(CuTSPc/C)_{700}$ sample, the ORR path on $(CuTSPc/C)_{700}$AL catalyst electrode is still the $4e^-$-dominated process, however, the electron transfer number is obviously decreased along with the largely increased H_2O_2 yield, particularly in the lower overpotential range; (iii) XRD and TEM analyses reveal that acid-leaching can remove effectively most of Cu. XPS results demonstrate that the central metal Cu ion not only is an important part for constructing the $(CuTSPc/C)_{700}$ catalyst ORR active sites, but also has a great effect on the stability of active N and S species.

Acknowledgements

The authors gratefully acknowledge financial support from the National Natural Science Foundation of China (21173039); International Academic Cooperation and Exchange Program of Shanghai Science and Technology Committee (14520721900); the Specialized Research Fund for the Doctoral Program of Higher Education, SRFD (20110075110001) of China, and College of Environmental Science and Engineering, State Environmental Protection Engineering Center for Pollution Treatment and Control in Textile Industry, Donghua University, Shanghai 201620, China. All the financial supports are gratefully acknowledged.

References

[1] S. Srinivasan, Fuel cells: from fundamentals to applications. New York: Springer, 2006.

[2] G. Hooger, Fuel cell technology handbook. Boca Raton: CRC Press, 2002.

[3] J. F. Wu, X. Z. Yuan, J.J. Martina, H. J. Wang, J. J. Zhang, J. Shen, S. H. Wu, W Merid, A review of PEM fuel cell durability: degradation mechanisms and mitigation strategies, J. Power Sources, 184 (2008) 104-119.

[4] M. P. Hogarth, T. R. Ralph, Catalysis for low temperature fuel cells, Platinum Metals Review, 46 (2002) 146-164.

[5] M. M. Mench, C. Y. Wang, S. T. Thynell, An introduction to fuel cells and related transport phenomena, Int. J. Transport Phenomena, 3 (2001) 151-176.

[6] F. Gloaguen, P. Convert, S. Gamburzev, O. A. Velev, S. Srinivasan, An evaluation of the macro-homogeneous and agglomerate model for oxygen reduction in PEMFCs, Electrochim. Acta. 43 (1998) 3767-3772.

[7] M. M. Matthew, C. Y. Wang, T. T. Stefan, A review of polymer electrolyte membrane fuel cells: technology, applications, and needs on fundamental research, Appl. Energy, 88 (2011) 981-1007.

[8] Y. W. Ou, H. Kumagai, F. X. Yin, S. Okada, H. Hatasawa, H. Morioka, K Takanabe, J. Kubota, K. Domen, Electrocatalytic Activity and Stability of M-Fe Catalysts Synthesized by Polymer Complex Method for PEFC Cathode, J. Electrochem. Soc., 158 (2011) B1491-B1498.

[9] J. H. Kim, I. Akimitsu, M. Shigenori, K. Nobuyuki, K. I. Ota, Catalytic activity of titanium oxide for oxygen reduction reaction as a non-platinum catalyst for PEFC, Electrochim. Acta, 52 (2007) 2492-2497.

[10] B. Wang, Recent development of non-platinum catalysts for oxygen reduction reaction, J. Power Sources, 152 (2005) 1-15.

[11] J. L. Qiao, L. Xu, Y. Y. Liu, P. Xu, J. J. Shi, S. Y. Liu, B. L. Tian. Carbon-supported co-pyridine as non-platinum cathode catalyst for alkaline membrane fuel cells, Electrochim. Acta, 96 (2013) 298-305.

[12] E. M. Sommer, L. S. Martins, J. V. C. Vargas, J. E. F. C. Gardolinski, J. C. Ordonez, C. E. B. Marino, Alkaline membrane fuel cell (AMFC) modeling and experimental validation, J. Power Sources, 2 (2012) 16-30.

[13] E. Gülzow, Alkaline fuel cells: a critical view, J. Power Sources, 61 (1996) 99-104.

[14] Z. W. Chen, H. Drew, A. P. Yu, L Zhang, J. J. Zhang, A review on non-precious metal electrocatalysts for PEM fuel cells, Energy & Environ. Sci., 4 (2011) 3167-3192.

[15] X. G. Li, C. P. Liu, W. Xing, T. H. Lu, Development of durable carbon black/titanium dioxide supported macrocycle catalysts for oxygen reduction reaction, J. Power Sources, 193 (2009) 470-476.

[16] P. S. Nalini, X. G. Li, N. Vijayadurda, P. K. Swaminatha, C. M. Hector, G. Wu, J. W. Lee, N. P. Branko, Nitrogen-modified carbon-based catalysts for oxygen reduction reaction in polymer electrolyte membrane fuel cells, J. Power Sources, 188 (2009) 38-44.

[17] A. Morozan, B. Jousselme, S. Palacin, Low-platinum and platinum-free catalysts for the oxygen reduction reaction at fuel cell cathodes, Energy & Environ. Sci., 4 (2011) 1238-1254.

[18] J. J. Shi, X. J. Zhou, P. Xu, J. L .Qiao, Z. W. Chen, Y. Y. Liu, Nitrogen and Sulfur Co-doped Mesoporous Carbon Materials as Highly Efficient Electrocatalysts for Oxygen Reduction Reaction, Electrochim. Acta, 145 (2014) 259-269.

[19] W. B. Cicero, L. Zhang, K. Lee, H. S. Liu, L B M Aldalea,P M Edmar, H. J. Wang, J. J. Zhang, A review of Fe-N/C and Co-N/C catalysts for the oxygen reduction reaction, Electrochim. Acta, 53 (2008) 4937-4951.

[20] J. L. Qiao, L. Xu, L. Ding, L. Zhang, R Baker, X. F. Dai, J. J. Zhang, Using pyridine as nitrogen-rich precursor to synthesize Co-N-S/C non-noble metal electrocatalysts for oxygen reduction reaction, Appl. Catal. B: Environ., 125 (2012) 197-205.

[21] I. Kruusenberg, L. Matisen, K. Tammeveski, Oxygen electroreduction on multi-walled carbon nanotube supported metal phthalocyanines and porphyrins in alkaline media, J. Nanosci. & Nanotech.,13 (2013) 621-627.

[22] L. Ding, X. Qing, .X J. Zhou, J. L. Qiao, H. Li, H. J. Wang, Electrochemical behavior of nanostructured nickel phthalocyanine (NiPc/C) for oxygen reduction reaction in alkaline media, J. Appl. Electrochem., 43 (2013) 43-51.

[23] G. Wu, L. Karren, M. J. Christina, Z. Piotr, High-performance electrocatalysts for oxygen reduction derived from polyaniline, iron and cobalt, Science, 332 (2011) 443-447.

[24] L. Ding, X. F. Dai, R. Lin, H. J. Wang , J. L. Qiao, Electrochemical performance of carbon-supported Co-phthalocyanine modified with Co-added metals (M= Fe, Co, Ni, V) for oxygen reduction reaction, J. Electrochem. Soc., 159 (2012) F577-F584.

[25] U. I. Kramm, I. Abs-Wurmbach, I. Herrmann-Geppert, J. Radnik, S. Fiechter, P. Bogdanoff, Influence of the electron-density of FeN4-centers towards the catalytic activityof pyrolyzed FeTMPPCl-based ORR-electrocatalysts, J. Electrochem. Soc., 158 (2011) B69-B78.

[26] P. Xu, W. Z. Chen, Q. Wang, T. S. Zhu, M. J. Wu, J. L. Qiao, Z. W. Chen, J. J. Zhang, Effects of transition metal precursors (Co, Fe, Cu, Mn, or Ni) on pyrolyzed carbon supported metal-aminopyrine electrocatalysts for oxygen reduction reaction, RSC Adv., 5 (2015) 6195-6206.

[27] Y. Nabae, S. Moriya, K Matsubayashi, S. M. Lyth, M. Malon, L. B. Wu, N. MIslam, Y. Koshigoe, S Kuroki, M. AKakimoto, S. Miyata, J. Ozaki, The role of Fe species in the pyrolysis of Fe phthalocyanine and phenolic resin for preparation of carbon-based cathode catalysts, Carbon, 48 (2010) 2613-2624.

[28] R. P. Baker, D. Wilkinson, J. J. Zhang, Electrocatalytic activity and stability of substituted iron phthalocyanines towards oxygen reduction evaluated at different temperatures, Electrochim. Acta, 53 (2008) 6906-6919.

[29] I. Kruusenberg, L. Matisen, Q. Shah, A. M. Kannan, K. Tammeveski, Non-platinum cathode catalysts for alkaline membrane fuel cells, Int. J. Hydrogen Energy, 37 (2012) 4406-4412.

[30] Z. P. Li, B. H. Liu, The use of macrocyclic compounds as electrocatalysts in fuel cells, J Appl. Electrochem., 40 (2010) 475-483.

[31] N. Sehlotho, T. Nyokong, Effects of ring substituents on electrocatalytic activity of manganese phthalocyanines towards the reduction of molecular oxygen. J. Electroanal. Chem., 595 (2006) 161-167.

[32] L. Ding, J. L. Qiao, X. F. Dai, J. Zhang, J. J .Zhang, B. L. Tian, Highly active electrocatalysts for oxygen reduction from carbon-supported copper-phthalocyanine synthesized by high temperature treatment, Int. J. Hydrogen Energy, 37 (2012) 14103-14113.

[33] X. Qing, J. J. Shi, C. Y. Ma, M. Y. Fan, Z. Y. Bai, Z. W. Chen, J. L. Qiao, J. J. Zhang, Simultaneous formation of nitrogen and sulfur-doped transition metal catalysts for oxygen reduction reaction through pyrolyzing carbon-supported copper phthalocyanine tetrasulfonic acid tetrasodium salt, J. Power Sources, 266 (2014) 88-98.

[34] L. Qu, Y. Liu, J. B. Baek, L.M. Dai, Nitrogen-doped graphene as efficient metal-free electrocatalyst for oxygen reduction in fuel cells, ACS Nano, 4 (2010) 1321-1326.

[35] L. P. Zhang, J.B. Niu, L. M. Dai, Z. H. Xia, Effect of microstructure of nitrogen-doped graphene on oxygen reduction activity in fuel cells, Langmuir, 28 (2012) 7542-7550.

[36] W. Xia, J. Masa, M. Bron, W. Schuhmann, M. Muhler, Highly active metal-free nitrogen-containing carbon catalysts for oxygen reduction synthesized by thermal treatment of polypyridine-carbon black mixtures, Electrochem. Commun. 13(6) (2011) 593-596.

[37] X.G. Li, B.N. Popova, T. Kawaharab, H. Yanagi, Non-precious metal catalysts synthesized from precursors of carbon, nitrogen, and transition metal for oxygen reduction in alkaline fuel cells, J. Power Sources, 196 (2011) 1717-1722.

[38] J. J. Shi, X. J. Zhou, P. Xu, J. L. Qiao, Z. W. Chen, Y. Y. Liu, Nitrogen and Sulfur Co-doped Mesoporous Carbon Materials as Highly Efficient Electrocatalysts for Oxygen Reduction Reaction, Electrochim. Acta, 145 (2014) 259–269.

[39] P. Justin, P. H. K. Charan, G. R. Rao, Activated zirconium carbide promoted Pt/C electrocatalyst for oxygen reduction, Appl. Catal. B: Environ., 144 (2014) 767-774.

[40] Y. J. Hu, H. Zhang, P. Wu, H. Zhang, B. Zhou, C. X. Cai, Bimetallic Pt-Au nanocatalysts electrochemically deposited on graphene and their electrocatalytic characteristics towards oxygen reduction and methanol oxidation, Phys. Chem. Chem. Phys., 13 (2011) 4083-4094.

[41] Q. Y. Liu, Z. Y. Liu, Z. P. Zhu, G. Y. Xie, Y. L. Wang, Al_2O_3-Coated honeycomb cordierite-supported CuO for simultaneous SO_2 and NO removal from flue gas: effect of Na_2O additive, Ind. & Eng. Chem. Res., 43 (2004) 4031-4037.

[42] X. G. Wen, W. X. Zhang, S. H. Yang, Z. R. Dai, Z. L. Wang, Solution phase synthesis of $Cu(OH)_2$ nanoribbon by coordination self-assembly using Cu_2S nanowires as precursors, Nano Lett., 2 (2002) 1397-1401.

[43] K. Xiao, R. J. Li, J. Tao, E. A. Payzant, I. N. Ivanov, A. A. Puretzky, W. P. Hu, D. B. Geohegan, Metastable copper-phthalocyanine single-crystal nanowires and their use in fabricating high-performance field-effect transistors, Adv. Funct. Mater. 19 (2009) 3776-3780.

[44] G. Soto, J. A. Díaz, W. D. L. Cruz, Copper nitride films produced by reactive pulsed laser deposition, Mater. Lett., 57 (2003) 4130-4133.

[45] S. Velu, K. Suzuki, M. Vijayaraj, S. Barman, C. S. Gopinath, In situ XPS investigations of Cu1-xNixZnAl-mixed metal oxide catalysts used in the oxidative steam reforming of bio-ethanol, Appl. Catal. B: Environ., 55 (2005) 287-299.

[46] T. B. Du, Y. Luo, V. Desai, The combinatorial effect of complexing agent and inhibitor on chemical-mechanical planarization of copper, Microelectron. Eng., 71 (2004) 90-97.

[47] S. L. Gojkovic, S. Gupta, R. F. Savinell., Heat-treated iron(III) tetramethoxyphenyl porphyrin chloride supported on high-area carbon as an electrocatalyst for oxygen reduction Part II. Kinetics of oxygen reduction, J. Electroanall Chem., 462 (1999) 63-72.

[48] Q. G. He, X. F. Yang, R. H. He, B. L. Agustín, M. Hamish, X. M. Ren, W. L. Yang, K. Bruce E, Electrochemical and spectroscopic study of novel Cu and Fe-based catalysts for oxygen reduction in alkaline media, J. Power Sources, 213 (2012) 169-179.

[49] K. C. Lee, L. Zhang, H. S. Liu, R. Hui, Z. Shi, J. J. Zhang, Oxygen reduction reaction (ORR) catalyzed by carbon-supportedcobalt polypyrrole (Co-PPy/C) electrocatalysts, Electrochim. Acta, 54 (2009) 4704-4711.

[50] V. Nallathambi, J. W .Lee, S. P. Kumaraguru, G. Wu, B. N. Popov, Development of high performance carbon composite catalyst for oxygen reduction reaction in PEM proton exchange membrane fuel cells, J. Power Sources, 183 (2008) 34-42.

[51] H. Gao, Z. Liu, L. Song, W. H. Guo, W. Gao, L. J. Ci, A. Rao, W. J. Quan, R. Vajtai, P. M. Ajayan, Synthesis of S-doped graphene by liquid precursor, Nanotechnology, 23 (2012) 1-7.

[52] Z. Liu, H. G. Nie, Z. Yang, J. Zhang, Z. P. Jin,Y. Q. Lu, Z. B. Xiao, M. H. Shao, Sulfur-nitrogen co-doped three-dimensional carbon foams with hierarchical pore structures as efficient metal-free electrocatalysts for oxygen reduction reactions, Nanoscale, 5 (2013) 3283-3288.

Figure captions

Fig. 1 (a) Polarization curves of ORR catalyzed by $(CuTSPc/C)_{700}$ and $(CuTSPc/C)_{700}AL$ catalysts in O_2-saturated 0.1M KOH solution. (b) Tafel plots of log j_k vs. E (V) for ORR catalyzed by $(CuTSPc/C)_{700}$ and $(CuTSPc/C)_{700}AL$ catalysts deduced from the polarization curves in (a). Scan rate: 5 mV s^{-1}. Electrode rotation rate: 1500 rpm. Catalyst loading: 505 μg cm^{-2}.

Fig. 2 (a) Rotating ring-disk electrode measurements for ORR catalyzed by $(CuTSPc/C)_{700}$ catalysts synthesized before and after acid-leaching at a scan rate of 5 mV s^{-1} in O_2-saturated 0.1M KOH solution, (b) The same as Fig. 1, (c) The corresponding $\%H_2O_2$ yield, and (d) electron transfer numbers of ORR catalyzed by the sample indicated. Catalyst loading: 505 μg cm^{-2}. Rotating rate: 1500 rpm.

Fig. 3 X-ray diffraction pattern of $(CuTSPc/C)_{700}$ and $(CuTSPc/C)_{700}AL$ catalysts.

Fig. 4 TEM images of (a) $(CuTSPc/C)_{700}$, (b) an enlargement of the area outlined in (a) and (c) $(CuTSPc/C)_{700}AL$.

Fig. 5 XPS spectra of (a) Cu 2p for $(CuTSPc/C)_{700}$, (b) Cu 2p for $(CuTSPc/C)_{700}AL$, (c) N 1s for $(CuTSPc/C)_{700}$, (d) N 1s for $(CuTSPc/C)_{700}AL$, (e) the content of each types of N for $(CuTSPc/C)_{700}$ and $(CuTSPc/C)_{700}AL$, (f) S 2p for $(CuTSPc/C)_{700}$, (g) S 2p for $(CuTSPc/C)_{700}AL$, (h) the content of each types of S for $(CuTSPc/C)_{700}$ and $(CuTSPc/C)_{700}AL$.

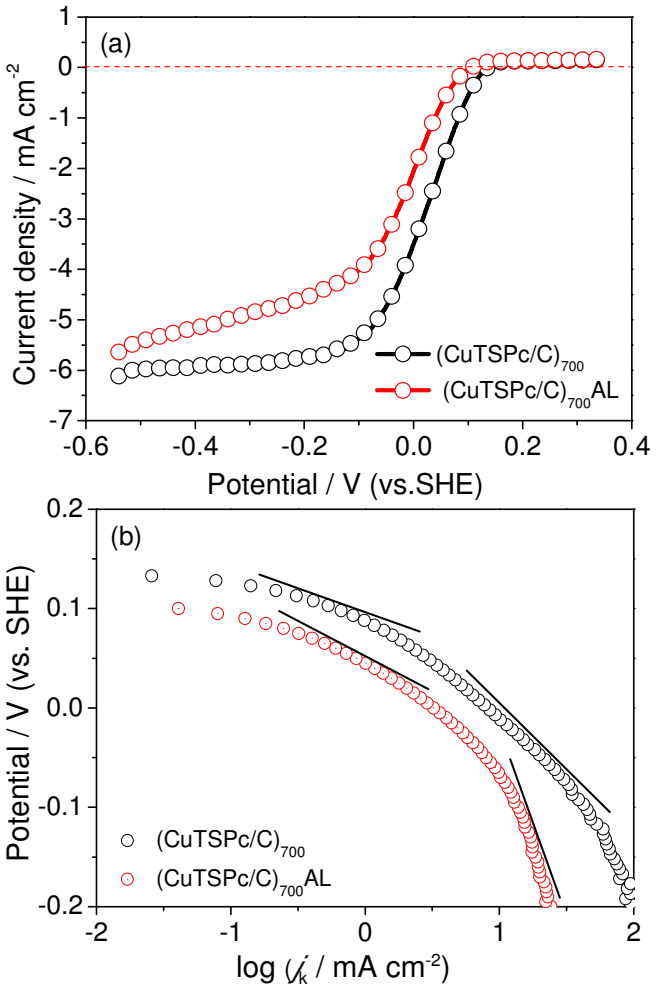

Fig. 1

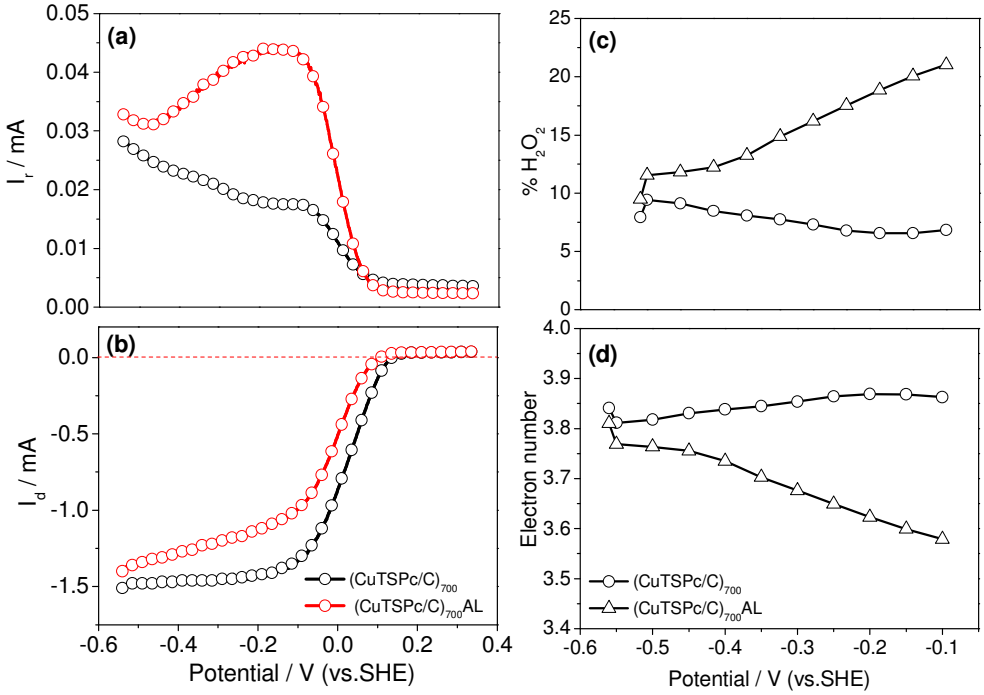

Fig. 2

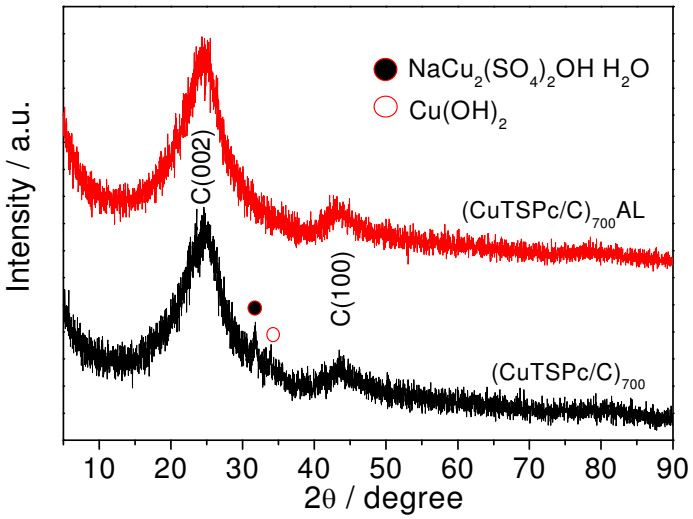

Fig. 3

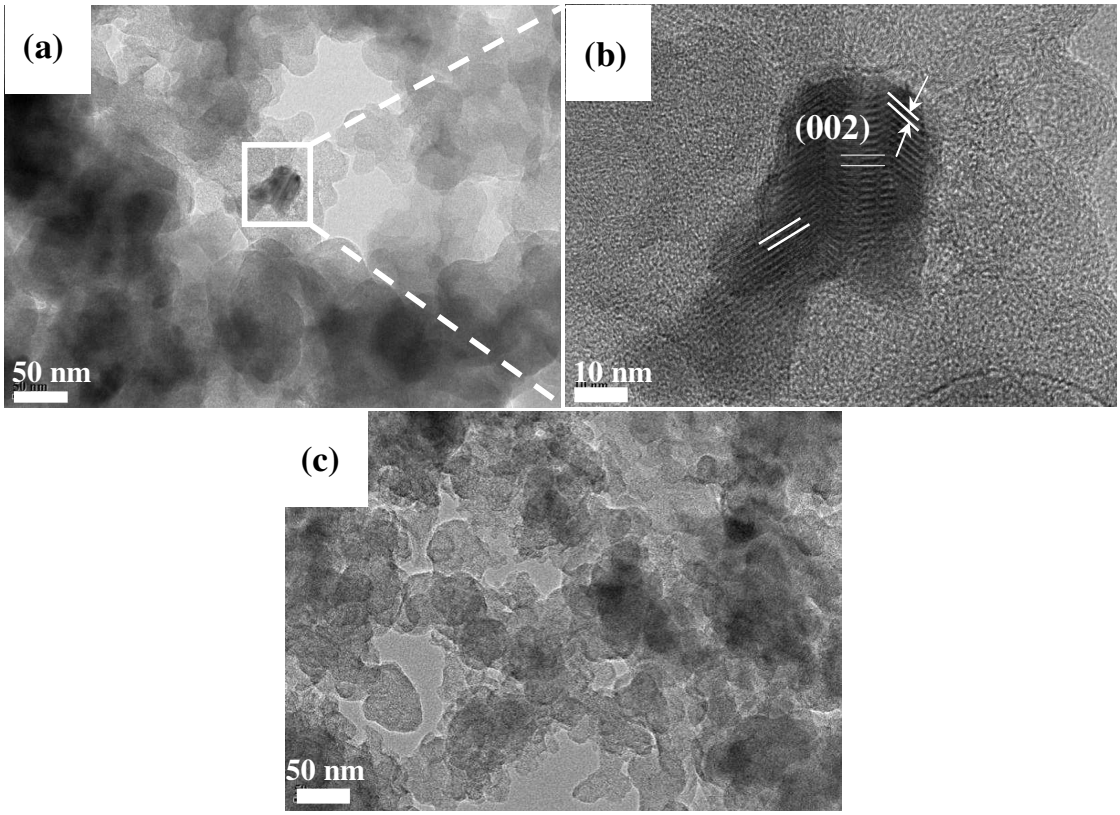

Fig. 4

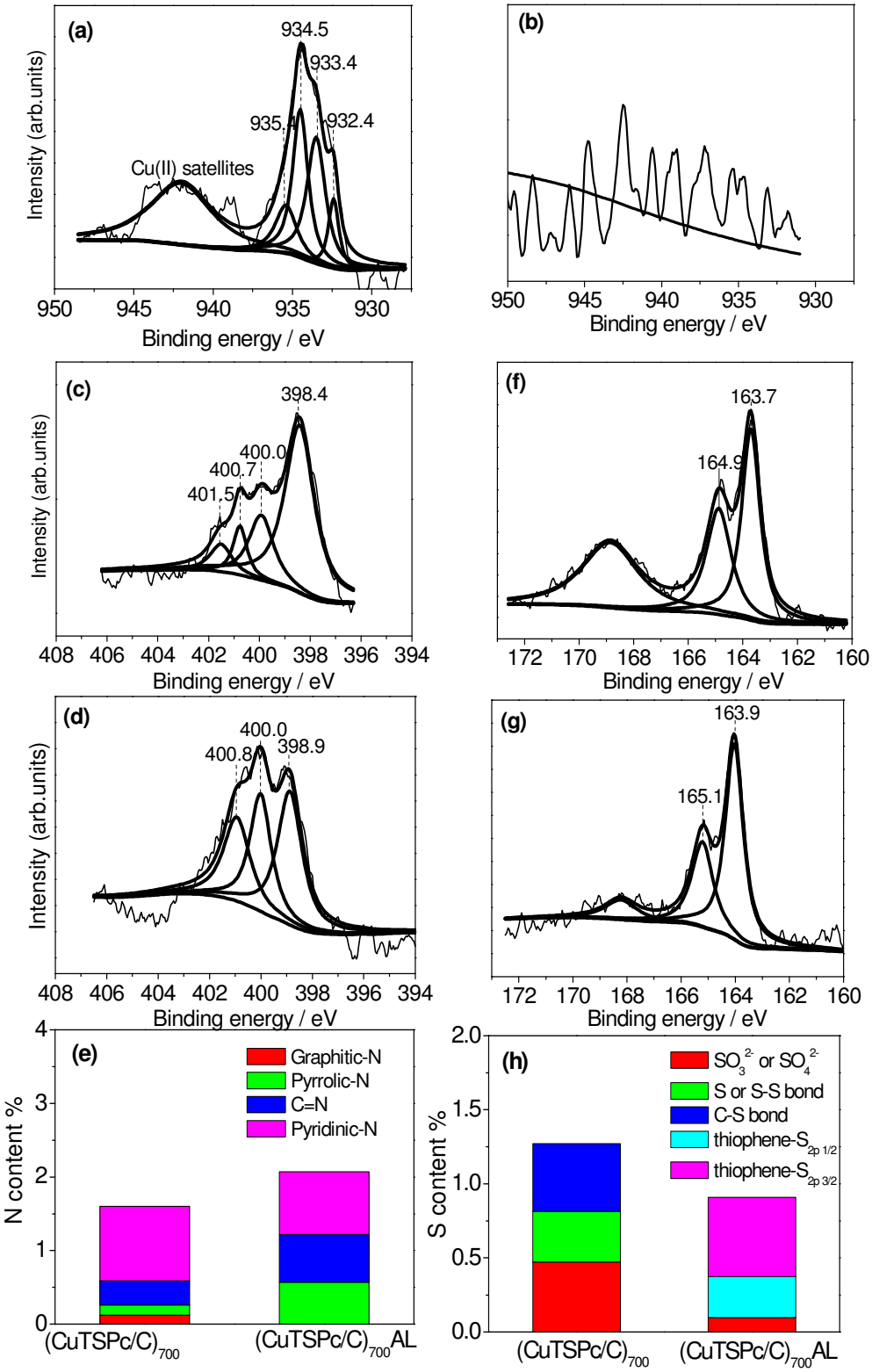

Fig. 5

Table 1 The content of elements for CuTSPc/C synthesized at different temperatures, determined by EDS.

Element	CuTSPc/C		$(CuTSPc/C)_{600}$		$(CuTSPc/C)_{700}$		$(CuTSPc/C)_{800}$	
	wt.%	at.%	wt.%	at.%	wt.%	at.%	wt.%	at.%
C	64.88	72.71	66.96	74.27	67.72	74.33	80.90	86.05
N	11.11	10.67	12.11	11.52	11.84	11.14	9.26	8.45
O	15.32	12.89	13.09	10.90	14.86	12.24	4.86	3.88
Na	3.00	1.75	3.01	1.75	1.86	1.07	0.24	0.13
S	3.69	1.55	2.71	1.13	2.20	0.91	2.75	1.10
Cu	2.00	0.42	2.11	0.44	1.52	0.31	1.99	0.40

Table 2 Concentrations (at%) of C, N, O, S and Cu in the $(CuTSPc/C)_{700}$ and $(CuTSPc/C)_{700}AL$ catalyst samples, determined by XPS.

Sample	C	N	O	S	Cu
$(CuTSPc)_{700}$	88.71	1.60	7.05	1.27	0.38
$(CuTSPc)_{700}AL$	88.63	2.07	8.40	0.91	—